Batteries & Supercaps

Research Article
doi.org/10.1002/batt.202500361

Chemistry Europe
European Chemical Societies Publishing

www.batteries-supercaps.org

Understanding the Role of Cathode Solubility in Magnesium Batteries: A Case Study of Substituted Bis-Benzoquinones

Alae Eddine Lakraychi, Leonard Linshin Jiang, Wen Ren, Ye Zhang, Yanliang Liang, Mark Wayne Lee Jr., and Yan Yao*

Rechargeable magnesium batteries (RMBs) have emerged as a promising alternative to lithium-ion batteries owing to their high energy density, enhanced safety, and cost-effectiveness. However, critical challenges remain for their commercial viability, particularly in the development of suitable cathode materials. In this study, substituted bis-benzoquinones as multielectron organic cathodes for magnesium batteries are investigated. These compounds are synthesized via a simple and scalable route, with competitive projected manufacturing costs. A systematic investigation of their solubility in magnesium-based electrolytes reveals a strong dependence on the chemical nature of the magnesium salt. Magnesium cells incorporating substituted bis-benzoquinones demonstrate high specific capacities of up to 419 mAh g^{-1} at an average voltage of 1.7 V versus Mg^{2+}/Mg, corresponding to a material-level specific energy of 600 Wh kg^{-1}. Furthermore, these compounds demonstrate excellent rate capability, delivering full capacity at 5C and retaining 70% of their capacity at 2 °C. These results underscore the potential of substituted bis-benzoquinones for cost-effective, high-energy, and fast-charging RMBs.

1. Introduction

Rechargeable magnesium batteries (RMBs) have emerged as promising candidates for post-lithium energy storage systems.[1,2] The use of a metallic magnesium anode offers several key advantages, including high energy density, enhanced safety, cost-effectiveness, and a more sustainable supply chain.[3,4] Since the pioneering work by Aurbach and colleagues in 2000,[5] significant progress has been made in understanding the fundamentals of Mg^{2+} storage and enhancing the practical feasibility of RMBs.[6] Notably, a variety of electrolyte solutions have been developed to enable reversible Mg deposition and dissolution, achieving ionic conductivities comparable to those of lithium-ion batteries.[7–11] Among these, halide-free magnesium salts featuring alkoxyborate and carborane anions in ether-based solvents enable reversible Mg stripping/plating with over 99% coulombic efficiency and anodic stability exceeding 3.5 V versus Mg^{2+}/Mg.[12,13] Moreover, their weakly coordinating anions also promote the uptake of bare Mg^{2+} into the cathode materials, thereby enhancing energy density.

On the cathode side, material selection remains a critical challenge,[14–16] as the direct adoption of intercalation hosts from lithium-based systems to magnesium batteries is impeded by the poor mobility of Mg^{2+} ions within the host structure,[17–21] resulting in significantly reduced electrochemical performance. Conversion-type cathodes, such as sulfur and iodine, circumvent the limitations of solid-state Mg^{2+} diffusion by operating via a dissolution-precipitation reaction pathway.[22–25] However, the formation of soluble intermediates, such as MgS_n and $Mg(I_3)_2$, poses significant challenges due to their chemical incompatibility with both magnesium metal and current collectors.[26–28]

Organic cathodes, owing to their charge-compensation-based storage mechanism, have demonstrated the ability to store various charge carriers regardless of their size or chemical nature.[29–32] Numerous organic materials have been reported for RMBs with appreciable operating voltages and high specific capacities.[33–38] Recently, our group reported an advancement in RMB cathode development using the intermediate soluble pyrene-4,5,9,10-tetraone (PTO) as the cathode.[39] Leveraging a heterogeneous dissolution-precipitation reaction pathway, PTO exhibited high material utilization with a capacity of 315 mAh g^{-1} and an unprecedented specific power of 30.4 kW kg^{-1}, making it a strong candidate for Mg^{2+} storage. This outstanding performance is attributed to efficient Mg^{2+} uptake in the liquid phase, which substantially enhances reaction kinetics.

A. Eddine Lakraychi, L. L. Jiang, Y. Yao
Department of Electrical and Computer Engineering
University of Houston
Houston, TX 77204, USA
E-mail: yyao4@central.uh.edu

A. Eddine Lakraychi, Y. Yao
Texas Center for Superconductivity at the University of Houston (TcSUH)
University of Houston
Houston, TX 77204, USA

W. Ren
Department of Chemical and Biomolecular Engineering
University of Houston
Houston, TX 77204, USA

Y. Zhang, Y. Liang
LiBeyond LLC
Houston, TX 77023, USA

M. W. Lee, Jr.
Twelfth Vertex LLC
Columbia, MO 65201, USA

Supporting information for this article is available on the WWW under https://doi.org/10.1002/batt.202500361

Research Article
doi.org/10.1002/batt.202500361
Chemistry Europe
European Chemical Societies Publishing

The concept of organic magnesium batteries holds considerable promise; however, their commercial viability has yet to be realized. For example, large-scale production of PTO is hindered by low yield and limited availability of precursor materials.[40–42] Furthermore, while cathode dissolution enhances reaction kinetics and material utilization, it adversely affects long-term cycling stability. A fundamental understanding of how cathode solubility impacts performance metrics is still lacking.

In this work, we address these challenges by investigating substituted bis-benzoquinones as potential organic cathodes for RMBs. We synthesized two substituted bis-benzoquinones and systematically examined their solubility in various magnesium electrolyte solutions, revealing a significant dependence on the chemical nature of magnesium salts. The bis-benzoquinone derivatives exhibited specific capacities of up to 419 mAh g^{-1} at an average operating voltage of 1.7 V *versus* Mg^{2+}/Mg, corresponding to a material-level specific energy of up to 600 Wh kg^{-1}. Additionally, both compounds exhibited outstanding rate capability, maintaining full capacity up to 5C and retaining 70% of capacity at 20C.

2. Results and Discussion

2.1. MBBQ and NBBQ as Organic Cathodes for Mg Batteries

Our current research focuses on developing multielectron organic cathodes capable of exhibiting reversible magnesiation and demagnesiation, offering high capacity and cost-effective synthesis. As a dimer of benzoquinone, bis-benzoquinone stands as a promising candidate for multielectron organic cathodes, with a theoretical capacity of 501 mAh g^{-1}, corresponding to the exchange of two Mg^{2+} per molecule. However, the synthesis of the unsubstituted bis-benzoquinone currently relies on C—C cross-coupling reactions followed by column chromatography for purification, which significantly increases the overall synthetic cost. In this study, we introduced two distinct substituents onto the bis-benzoquinone molecule for the ease of synthesis and solubility tuning in the magnesium electrolyte (**Figure 1**a). Methyl groups were incorporated to produce 5,5′-dimethyl-2,2′-bi-*p*-benzoquinone (MBBQ) to enhance solubility, whereas acetamido groups were introduced to obtain 5,5′-acetamido-2,2′-bi-*p*-benzoquinone (NBBQ) to reduce solubility. With respect to electrochemical storage, both MBBQ and NBBQ may uptake two Mg^{2+} per molecule, delivering theoretical capacities of 440 and 328 mAh g^{-1}, respectively. Magnesium storage is expected to proceed via a dissolution-precipitation reaction pathway: the pristine (0% depth of discharge, DoD) and intermediate (50% DoD) states are partially soluble in the electrolyte to varying extents, while the fully discharged state (100% DoD) precipitates (Figure 1b).

2.2. Synthesis of MBBQ and NBBQ

Both MBBQ and NBBQ were synthesized in high yield using a straightforward approach based on a previously reported

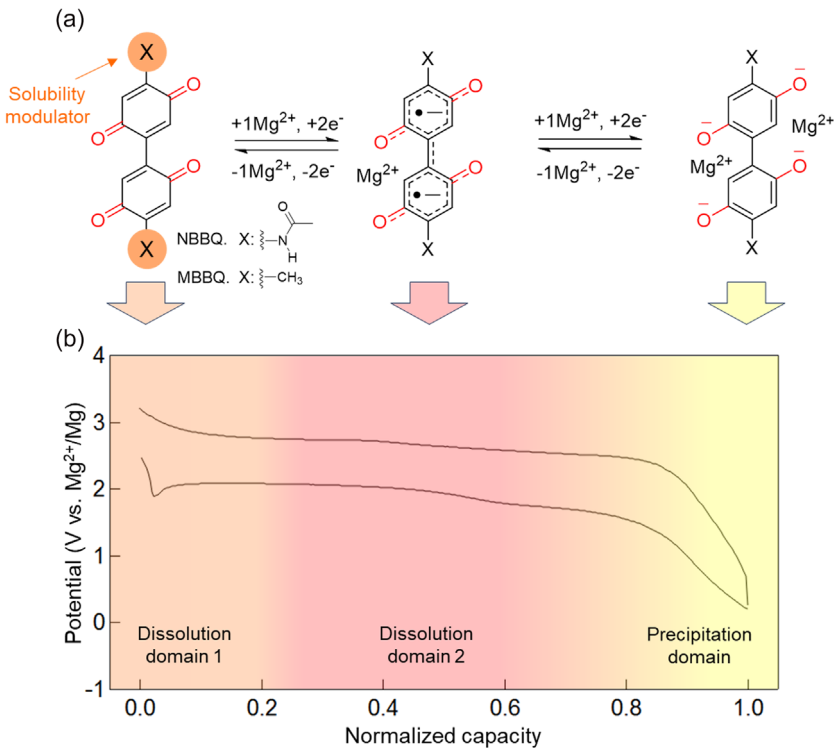

Figure 1. Multielectron bis-benzoquinone as an organic cathode for magnesium batteries. a) Proposed electrochemical reaction pathway bis-benzoquinone functionalized with methyl groups (MBBQ) and acetamido groups (NBBQ). b) Voltage profile of MBBQ cycled in $Mg(CB_{11}H_{12})_2$/G4 at 1C, illustrating the dissolution-precipitation mechanism. Distinct dissolution domains are marked to highlight the difference in solubility between the two regions.

Research Article
doi.org/10.1002/batt.202500361
Chemistry Europe
European Chemical Societies Publishing

method by Love et al. (**Figure 2**a).[43] In brief, an organic solution of the dimethoxybenzene derivative was added to an aqueous solution of ceric ammonium nitrite (CAN), resulting in immediate precipitation of the corresponding bis-benzoquinone product. The reaction completes within 4 h, and the product can be isolated by filtration, washed with water, and drying. Notably, this synthetic procedure is readily scalable, allowing for preparing batches of up to 100 g without compromising yield or extending reaction time.

The successful formation of the substituted bis-benzoquinones was confirmed via IR spectroscopy, with characteristic carbonyl (C═O) stretching bands observed in the 1620–1670 cm^{-1} range. Additional absorption bands were observed at 2900–3200 and 3300 cm^{-1}, corresponding to C—H and N—H stretching modes, indicative of methyl (—CH_3) and amine (—NH—) functional groups in MBBQ and NBBQ, respectively (Figure 2b). The resulting powders exhibit good crystallinity (Figure 2c) and consist of rod-shaped particles in the range of 15–20 μm in length and 1–5 μm in width (Figure 2d).

To evaluate the economic viability of these materials, we estimated manufacturing costs using the model proposed by Gregory et al.[44] (see Supplementary Text 1, Table S1–S4, Supporting Information, Figure S1 and S2, Supporting Information). The original methoxybenzene precursors employed in the syntheses described above are not suitable for large-scale production due to limited commercial availability in bulk quantities. To address

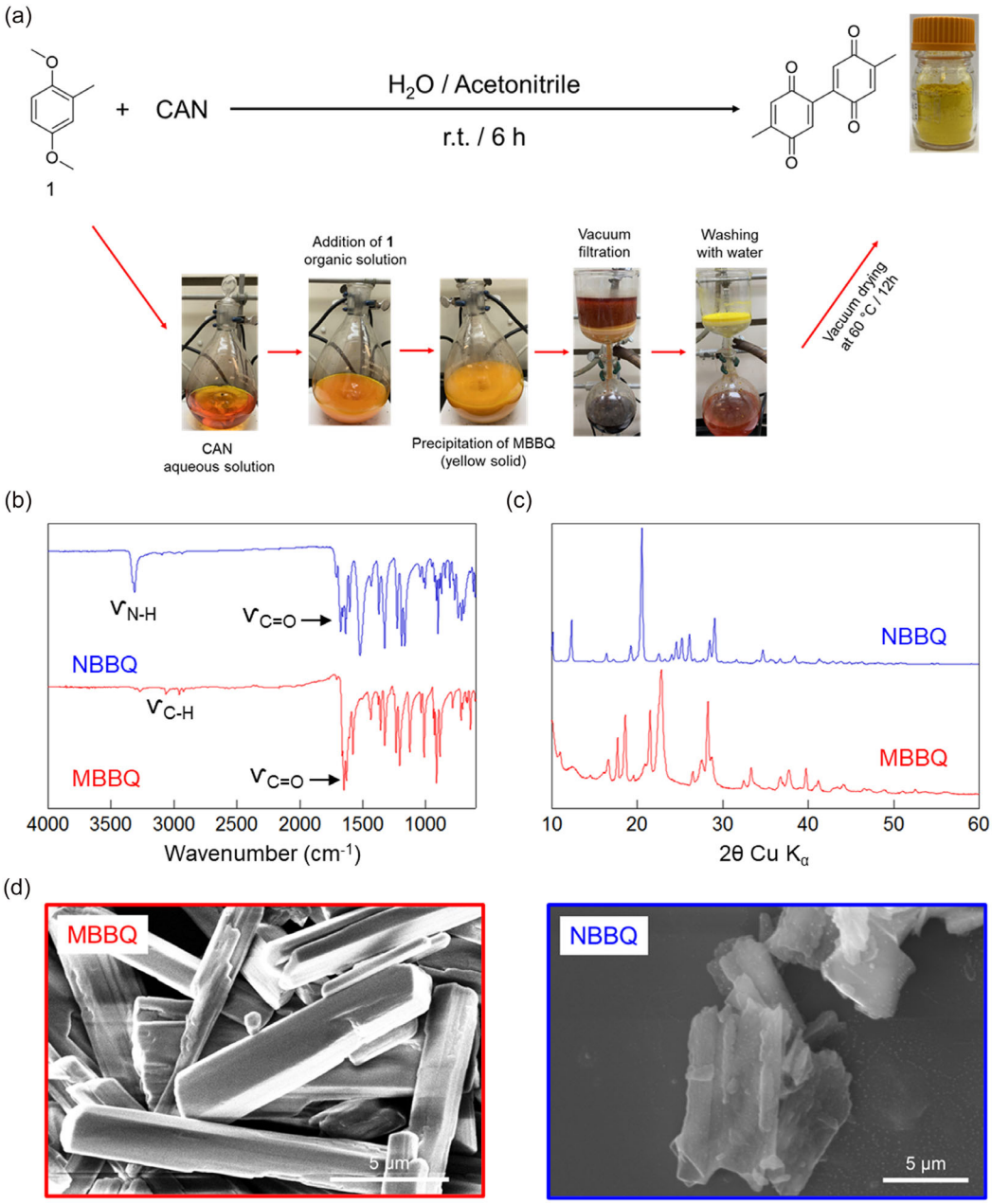

Figure 2. Synthesis and characterization of MBBQ and NBBQ. a) Stepwise synthetic procedure for a 100 g batch of MBBQ. Identical synthetic procedure was used for the synthesis of NBBQ using 2′,5′-dimethoxyacetanilide as the starting material. b–d) Corresponding IR spectra, PXRD patterns, and SEM images, respectively.

Research Article
doi.org/10.1002/batt.202500361
Chemistry Europe
European Chemical Societies Publishing

this, *m*-cresol—a coal tar-derived and readily available precursor—was selected for the synthesis of dimethoxytoluene, while 2,5-dimethoxyaniline was selected to produce dimethoxyacetanilide. Furthermore, to mitigate the high cost of CAN, an in-house synthesis using cerium hydroxide ($Ce(OH)_4$) was considered.

As illustrated in the block flow diagram (Figure S1, Supporting Information), MBBQ can be synthesized on a large scale via a three-step process with an overall yield of 49%, while NBBQ can be produced through a two-step synthetic route with an estimated overall yield of 70% (Figure S2, Supporting Information). According to the model's assumptions, the projected manufacturing costs are approximately $34/kg for MBBQ and $18/kg for NBBQ. While these estimates are subject to fluctuations in precursor and reagent prices, the projected costs are comparable to those of current state-of-the-art lithium-ion cathode materials and could be further reduced through efficient recycling and regeneration of CAN.

2.3. Solubility in Magnesium Electrolytes

The solubility of MBBQ and NBBQ was examined in two ether-based electrolyte formulations: a 1:1 v/v mixture of diglyme (G2) and 1,2-dimethoxyethane (DME) and tetraglyme (G4). To assess the effect of different anions, a range of magnesium salts was investigated, including the carborane-based $[Mg(CB_{11}H_{12})_2]$, alkyloxyborate-based $[Mg(B(hfip)_4)_2]$, and sulfonimide-based $[Mg(TFSI)_2]$ salts. For comparative analysis, the solubility of other intermediately soluble, conversion-type cathodes—such as PTO, sulfur, and iodine—was also assessed under the same electrolyte formulations. Solubility was quantified using UV-vis spectroscopy by correlating solute concentration with solution absorbance at a characteristic wavelength (Figure S3–S7, Supporting Information).

The measured solubilities (**Figure 3**a,b) reveal that the solubility of substituted bis-benzoquinones is influenced by two primary factors: the substituents on the bis-benzoquinone backbone and the magnesium salt in the electrolyte. Notably, MBBQ exhibited solubility values two orders of magnitude higher than those of NBBQ across all electrolyte formulations (**Table 1**). This substantial difference is attributed to the polarity of the substituents: nonpolar methyl groups enhance solute-solvent interactions, increasing the solubility of MBBQ, whereas polar acetamido groups favor intermolecular hydrogen bonding, which reduces solubility. These trends are consistent with observations of other methyl- or amine- substituted quinone derivatives.[45–47] Furthermore, MBBQ's solubility is approximately one order of magnitude lower than that of iodine, while NBBQ's solubility is slightly below that of PTO and comparable to that of sulfur.

In contrast, the influence of solvent itself appears to be minor. Solubility values remain within the same order of magnitude when G2/DME is replaced with G4, manifesting only slight decreases regardless of the salt used. For example, MBBQ's solubility decreases only slightly from 244 mM in G2/DME to 224 mM

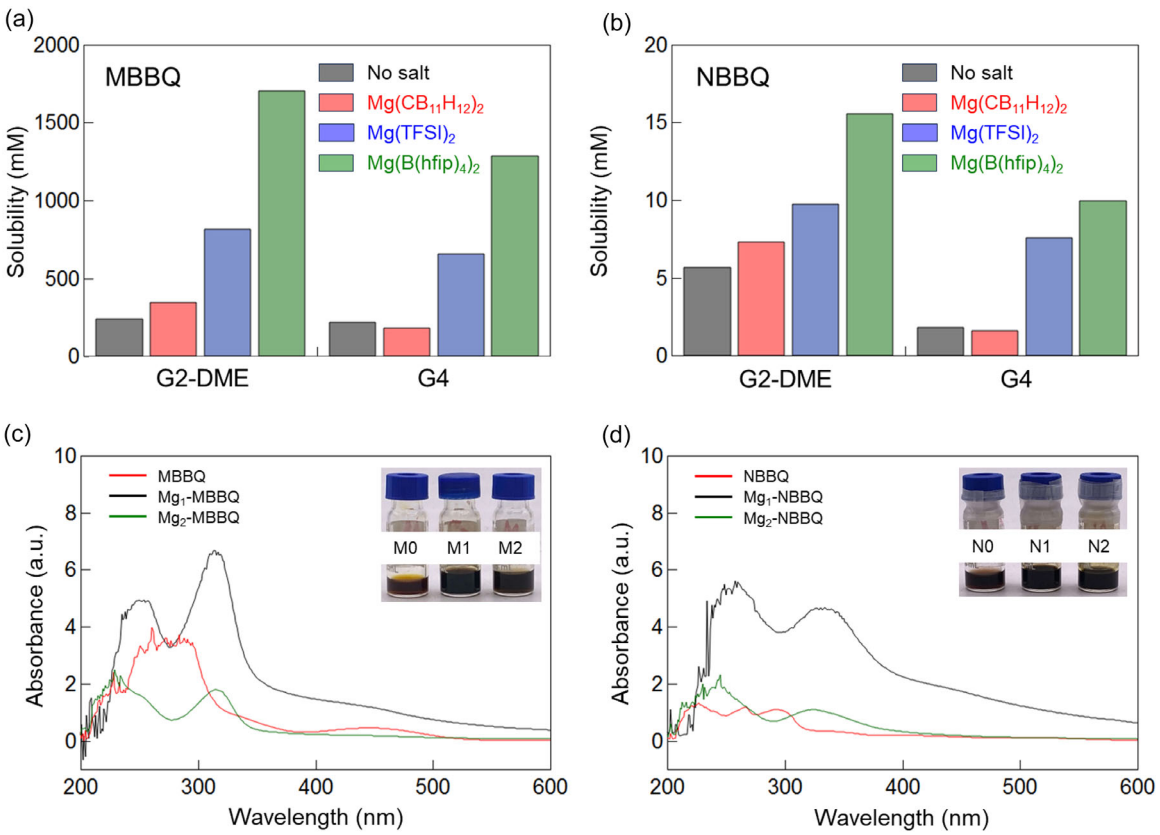

Figure 3. Solubility of MBBQ and NBBQ in various magnesium electrolytes. a,b) Solubility of MBBQ and NBBQ in G2-DME and G4 electrolyte formulations with various magnesium salts, respectively. c,d) UV-vis absorption spectra of saturated solutions of Mg_x-MBBQ and Mg_x-NBBQ (x = 0, 1, 2) in 0.45 M $Mg(CB_{11}H_{12})_2$/G2-DME electrolyte. M0, M1, M2, N0, N1, and N2 refer to MBBQ, Mg_1-MBBQ, Mg_2-MBBQ, NBBQ, Mg_1-NBBQ, and Mg_2-NBBQ, respectively.

Table 1. Solubility (mM) of MBBQ, NBBQ, PTO, sulfur, and iodine in various solvents and magnesium electrolyte formulations.

Solubility [mM]	G2-DME	$Mg(CB_{11}H_{12})_2$ G2-DME	$Mg(TFSI)_2$ G2-DME	$Mg(B(hfip)_4)_2$ G2-DME	G4	$Mg(CB_{11}H_{12})_2$ G4	$Mg(TFSI)_2$ G4	$Mg(B(hfip)_4)_2$ G4
MBBQ	244.00	350.00	818.00	1710.00	224.00	185.00	661.00	1289.00
NBBQ	5.70	7.36	9.77	15.60	1.86	1.62	7.60	10.12
PTO	13.92	43.29	51.19	60.76	11.92	29.20	48.43	55.23
Sulfur	11.80	10.04	0.23	2.93	5.97	5.71	0.45	3.14
Iodine	5400.00	1600.00	1600.00	5300.00	5800.00	4700.00	3600.00	6000.00

in G4. Although modest, this trend shows an inverse correlation with the dipole moment of the solvents (1.71 D for DME, 1.97 D for G2, and 2.45 D for G4).

Interestingly, the choice of magnesium salt exhibits pronounced effects on the solubility of both MBBQ and NBBQ, resulting in differences of up to one order of magnitude. For example, in G2/DME, the solubility of MBBQ increases from 350 mM with $[CB_{11}H_{12}]^-$ to 818 mM with $[TFSI]^-$ and further to 1710 mM with $[B(hfip)_4]^-$. This trend is consistent in G4 and also observed for NBBQ and PTO in both electrolyte systems. However, sulfur and iodine follow a different trend. These findings suggest that the solubility of MBBQ and NBBQ is primarily governed by weak interactions between the organic molecules and the electrolyte anions—likely electrostatic in nature—between polar functional groups (e.g., carbonyls or amides) and the anions. These interactions may influence the conformation and orientation of the quinones in solution. Such modulation of solubility by anion chemistry has also been reported by Pedraza et al.,[48] where the solubility of 2,2,6,6-tetramethylpiperidine-1-oxyl (TEMPO) in water increased by five orders of magnitude in the presence of $[TFSI]^-$ anions.

The above solubility corresponds to the pristine state (0% depth of discharge, DoD). However, for intermediately soluble quinone-type cathodes, the half-discharge state (50% DoD) typically represents the most soluble form.[49,50] For qualitative assessment, Mg_x-MBBQ and Mg_x-NBBQ (where $\times = 1$, 2) were prepared from their lithiated analogues via cation exchange in $Mg(CB_{11}H_{12})_2$/G2-DME. The resulting solutions were used as saturated solutions for UV-vis spectroscopy measurements.

The absorption spectra of the magnesiated intermediates (Figure 3c,d) reveal distinct features compared to the pristine states (0% DoD), confirming the formation of new molecular species. The similarity between the spectra of Mg_1-MBBQ (50% DoD) and Mg_2-MBBQ (100% DoD) may be attributed to residual Mg_1-MBBQ and the poor solubility of Mg_2-MBBQ. This residual Mg_1-MBBQ likely originates from incomplete conversion during the magnesiation of Li_4-MBBQ. A similar rationale applies to the residual Mg_1-NBBQ. As anticipated, Mg_1-MBBQ exhibits significantly higher absorbance than both pristine MBBQ and Mg_2-MBBQ, indicating that Mg_1-MBBQ is the most soluble species. A similar trend is observed for Mg_1-NBBQ, aligning with previously findings for Mg_1-PTO, Mg_xPSs, and $Mg(I_3)_2$ in magnesium electrolytes.[25,26,39]

2.4. Electrochemical Performance

To evaluate the intrinsic electrochemical properties of MBBQ and NBBQ at the molecular level, liquid-phase cyclic voltammetry (CV) was first conducted in a 0.1 M tetra-n-butylammonium perchlorate ($TBAClO_4$) solution in acetonitrile. The resulting cyclic voltammograms are shown in **Figure 4**a,c. During the initial cycle, both compounds exhibit multiple sequential redox events that evolve into four distinct redox waves in subsequent cycles, corresponding to the reversible electrochemical reduction and oxidation of four carbonyl groups per molecule. The additional redox features in the first cycle may arise from irreversible decomposition of residual impurities from synthesis. Half-wave potentials, determined by averaging the cathodic and anodic peak potentials, are summarized in Table S5, Supporting Information.

A comparison of the first redox event reveals a redox potential of −0.731 V versus Fc^+/Fc for NBBQ, which shifts to −0.844 V versus Fc^+/Fc for MBBQ. This shift reflects the strong electron-donating effect of the methyl substituents in MBBQ (Table S5, Supporting Information). The peak potential separation (ΔE_p) at a scan rate of 100 mV s^{-1} suggests moderate electrochemical reversibility: ΔE_p ranges from 90 to 180 mV for MBBQ and 90–100 mV for NBBQ.[51] These values are larger than those of PTO, a difference likely due to the twisted structure of bis-benzoquinone, which limits its intramolecular electron delocalization compared to the planar configuration of PTO.[52] Furthermore, the four redox waves show unequal peak areas, with waves I/I′ and II/II′ being more prominent than III/III′ and IV/IV′ smaller. This difference maybe due to the limited solubility of the tetraanion species, which could precipitate onto the glassy carbon electrode surface.[53,54]

The solid-state electrochemical performance of MBBQ and NBBQ was evaluated using galvanostatic cycling with a voltage range of 0.2−3.2 V versus Mg^{2+}/Mg at a cycling rate of 1C. A 0.45 M $Mg(CB_{11}H_{12})_2$ in G4 electrolyte was used to minimize solubility and enhance cycle stability. The resulting voltage profiles (Figure 4b,d) indicate a reversible magnesiation/demagnesiation process, characterized with the presence of flat plateaus and sloped regions. These features are further resolved in differential capacity (dQ/dV) plots, which show two major, reversible redox peaks (I/I′ and II/II′) (Figure 4e,f). The larger peak separation observed for MBBQ likely reflects its higher solubility in the electrolyte.

Both MBBQ and NBBQ achieve high material utilization exceeding 95%, corroborating the reversible reduction of four carbonyl groups per molecule in the solid phase. MBBQ delivers a specific capacity of 419 mAh g^{-1} at an average discharge voltage of 1.72 V versus Mg^{2+}/Mg, corresponding to a material-level specific energy of 600 Wh kg^{-1}. NBBQ, in comparison, achieves a specific capacity of 320 mAh g^{-1} with an average voltage of 1.71 V versus Mg^{2+}/Mg, resulting in a material-level specific energy of 475 Wh kg^{-1}. Previous reports on MBBQ in lithium-based cells indicated a limitation to three-electron redox activity per molecule,[47,55] attributed to the energetic instability of the tetraanion $MBBQ^{4-}$ as predicted

Research Article
doi.org/10.1002/batt.202500361
Chemistry Europe
European Chemical Societies Publishing

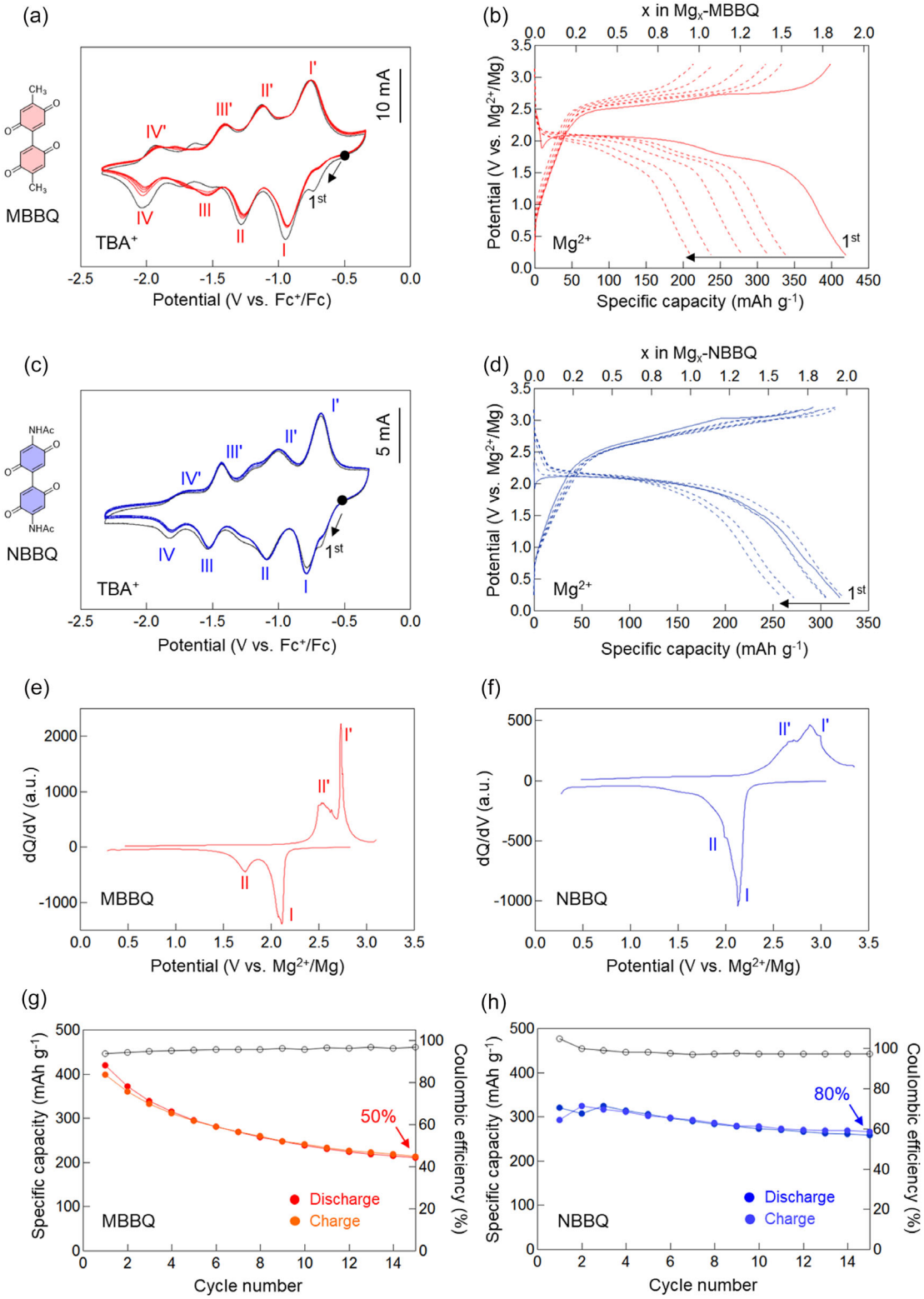

Figure 4. Electrochemical performance of MBBQ and NBBQ cells with magnesium anodes. a,c) Cyclic voltammograms of 1 mM MBBQ and NBBQ, respectively, in a three-electrode cell setup using 0.1 M tetra-n-butylammonium perchlorate in acetonitrile. Black circles indicate the open circuit potential, with 1st cycle represented by a solid line. b,d) Galvanostatic voltage profiles of MBBQ and NBQQ of cells using magnesium anodes and a 0.45 M $Mg(CB_{11}H_{12})_2$/G4 electrolyte at 1C (1C = 440 mA g^{-1} for MBBQ, and 1C = 326 mA g^{-1} for NBBQ). Profiles include selected cycles: 1st (solid line), 2nd, 3th, 5th, 10th, 15th. e,f) Corresponding dQ/dV versus potential for MBBQ and NBBQ during the first cycle. g,h) Corresponding cycling stability and coulombic efficiency.

by density functional theory (DFT) calculations.[47] Our results suggest that Mg^{2+} may stabilize $MBBQ^{4-}$, potentially via chelation, a hypothesis that warrants further exploration.

In terms of cycling stability, the two compounds exhibit distinct capacity retention profiles (Figure 4g,h). NBBQ retains 80% of its initial capacity after 15 cycles, whereas MBBQ retains only 50% due to active material loss, underscoring the detrimental effect of higher solubility on cycling stability. However, both compounds exhibit comparable coulombic efficiencies (94–96%), likely due to differences in solubility at varying DoD. To investigate the influence of electrolyte anion chemistry, additional cycling experiments were conducted using a 0.25 M $Mg(B(hfip)_4)_2$ in G4 electrolyte (Figure S8, Supporting Information). Under these conditions, both compounds exhibit reduced electrochemical performance and lower coulombic efficiency. MBBQ demonstrates a lower capacity of 386 mAh g^{-1}, corresponding to a material utilization of 87%, at an average discharge voltage of 1.67 V, resulting in a specific energy of 539 Wh kg^{-1} and a capacity retention of 56% after 15 cycles. NBBQ maintained a comparable capacity of 328 mAh g^{-1} with an average discharge voltage of 1.68 V, yielding a specific energy of 480 Wh kg^{-1}, though its capacity retention declines to 60% after 15 cycles.

Rate performance was also evaluated using 0.45 M $Mg(CB_{11}H_{12})_2$ in G2/DME, selected for its high ionic conductivity (Figure S9, Supporting Information).[39] Interestingly, both compounds maintain full material utilization at rates up to 5C. Even at a high C-rate of 20C, they retained 70% of their capacities, demonstrating excellent rate performance. These results are consistent with prior findings for PTO,[39] and highlight the advantage of intermediately soluble organic cathodes for fast-charging magnesium battery applications.

3. Conclusions

In conclusion, we evaluated two substituted bis-benzoquinones as promising multielectron organic cathodes for magnesium batteries. Both compounds were synthesized via a straightforward, and scalable route, with projected manufacturing costs that are competitive with current Li-ion cathodes. Our study reveals that cathode solubility—and consequently cycling stability—is strongly influenced by the nature of the substituents on the bis-benzoquinone backbone and the choice of electrolyte anion. The compounds exhibited specific capacities of up to 419 mAh g^{-1} at an average operating voltage of 1.7 V *versus* Mg^{2+}/Mg, corresponding to a material-level specific energy of up to 600 Wh kg^{-1}. Furthermore, they exhibited excellent rate capabilities, retaining full capacity at rates up to 5C and 70% capacity at 20C, highlighting their potential for fast-charging magnesium battery applications.

4. Experimental

Materials and Methods

The following chemicals and solvents were purchased from commercial suppliers and used without further purification: 1,4-dimethoxytoluene and 2′,5′-dimethoxyacetanilide from TCI chemicals; CAN, anhydrous diglyme (G2), anhydrous tetraglyme (G4), anhydrous dimethoxyethane (DME), and tetra-n-butylammonium perchlorate (TBAP) from Sigma Aldrich; and anhydrous acetonitrile and ferrocene from Alfa Aesar.

Attenuated total reflectance-Fourier transform infrared (ATR-FTIR) spectra were recorded on a Thermo Scientific Nicolet iS5 spectrometer. ^{1}H NMR spectra were recorded on JEOL ECA-500 MHz spectrometers. Chemical shifts are reported in ppm (δ) with the residual signals of deuterated solvents used for calibration. UV-vis spectra were recorded on Agilent Cary 60 spectrometer. Powder X-ray diffraction (PXRD) patterns were obtained using Rigaku MiniFlex 600 with Cu Kα radiation ($\lambda = 1.5406$ Å) operating at 40 kV − 15 mA. The data were recorded in 2θ range of 5–60° with a step width of 0.01° and a scan rate of 1.8° min^{-1}.

Materials and Methods: Synthesis of 5,5′-Dimethyl-2,2′-Bi-P-Benzoquinone (MBBQ)

Ten grams (66 mmol) of 1,4-dimethoxytoluene was dissolved in 250 mL of acetonitrile and was treated with an aqueous solution of 133 g (242 mmol) of CAN in 250 mL of deionized water at room temperature for 4 h. The obtained orange precipitate was filtered off, washed with deionized water, and then vacuum dried at 70 °C overnight. The resulting yellow powder is MBBQ. Yield: 85%. A similar procedure was adopted to produce 100 g of MBBQ with a similar yield. ^{1}H NMR ($CDCl_3$): δ 6.82 (s, 2H), 6.71 (d, 2H), 2.11 (d, 6H). $\tilde{\upsilon} = 3269, 3062, 2954, 1646, 1626, 1527, 1432, 1373, 1232, 1203, 1122, 1033, 1009, 927, 883, 715, 640$ cm^{-1}.

Materials and Methods: Synthesis of 5,5′-Acetamido-2,2′-bi-p-Benzoquinone (NBBQ)

Five grams (25 mmol) of commercial 2′,5′-dimethoxyacetanilide was dissolved in 125 mL of acetonitrile and was treated with an aqueous solution of 51 g (93 mmol) of CAN in 125 mL of deionized water at room temperature for 4 h. The obtained orange precipitate was filtered off, washed with deionized water and then vacuum dried at 70 °C overnight. The resulting yellow powder is NBBQ. Yield: 70%. A similar procedure was adopted to produce 100 g of NBBQ with similar yield. ^{1}H NMR (DMSO-d_6): δ 9.87 (s, 2H), 7.47 (s, 2H), 6.96 (s, 2H), 2.21 (s, 6 H). $\tilde{\upsilon} = 3309, 1671, 1657, 1633, 1600, 1518, 1369, 1322, 1223, 1187, 1162, 899, 739, 710, 595$ cm^{-1}.

Materials and Methods: Synthesis of Mg_x-MBBQ and Mg_x-NBQQ

MBBQ powders were reacted with a stoichiometric amount of lithium naphthalene solution in anhydrous DME overnight. The obtained mixture was then filtered off, washed with DME, and then dried under vacuum at 120 °C to yield Li_x-MBBQ (x = 2, 4). Subsequently, 50 mg of the as-obtained Li_x-MBBQ powders were dissolved in 400 μL of $Mg(CB_{11}H_{12})_2$/G2-DME electrolyte and stirred at room temperature for 1 week. The resulting mixture was filtered to obtain Mg_x-MBBQ as a saturated solution for UV-vis measurements. A similar procedure was employed to produce the saturated solution of Mg_x-NBBQ.

Materials and Methods: Solubility Measurement

Saturated solutions of MBBQ, NBBQ, PTO, sulfur, and iodine were prepared by dissolving 10 to 300 mg powder in 500 μL of each electrolyte solution, followed with continuous stirring overnight. The electrolyte solutions used included 0.45 M of $Mg(CB_{11}H_{12})_2$ in G2-DME or G4, 0.25 M of $Mg[B(hfip)_4]_2$ in G2-DME or G4,[13] and 0.5 M

of $Mg(TFSI)_2$ in G2-DME or G4. The mixtures were filtered off through Millipore PVDF 0.21 μm filters to remove any undissolved solids after 24 h. The saturated solutions were then subjected to dilution, with dilution factors of 60, 60, 60, 50, and 200 for MBBQ, NBBQ, PTO, sulfur, and iodine, respectively. To establish calibration curves, five standard solutions with various mass concentrations were prepared from the stock solutions for each material. Absorbance measurements were conducted across the 200–800 nm range. The calibration curves were constructed by correlating the maximum absorbance of 445 nm, 399 nm, 380 nm, 264 nm, and 456 nm for MBBQ, NBBQ, PTO, sulfur, and iodine, respectively, with the corresponding material concentrations in standard solutions using the Beer-Lambert law: $A = \varepsilon lC$ (A: absorbance; ε: molar extinction coefficient; l: length of the cell; C: material concentration).

Materials and Methods: Electrochemistry

CV was performed with a Biologic Science Instrument (VMP3). A three-electrode cell setup with a glassy carbon working electrode (3 mm diameter, CH instruments), platinum wire counter electrode (CH instruments), a silver wire pseudo-reference-electrode, and an electrolyte consisting of 0.1 M tetra-n-butylammonium perchlorate in anhydrous acetonitrile were used for measurements. Typically, 1 mM of active material was dissolved in the electrolyte solution. The voltammograms were recorded inside a glovebox at a scan rate of 100 mV s^{-1} and at room temperature. Ferrocene was added to the solution after testing and used as an internal reference.

Magnesium cell assembly and electrochemical measurements. The active material, Ketjenblack carbon (KB), and polytetrafluoroethylene (PTFE) binder were mixed in a 3:5:2 mass ratio using an agate mortar for 20 min, with the aid of isopropanol to enhance mixing and malleability. The resulting rubber-like composite electrode was calendared, dried in air for 6 h, and then dried under vacuum at 70 °C for overnight. Afterwards, the self-standing composite electrode was cut into discs of diameter 3/16-inch, with a typical areal mass loading of 2 mg cm^{-2}. Swagelok cells were assembled in an mBraun argon-filled glovebox, using the composite electrodes as cathodes, polished magnesium foil (3/16-inch diameter, 90 μm thickness) as the anode, and glass fiber separator (Whatman, Grade GF/A, 7/16-inch) impregnated with 150 μL of electrolyte (corresponding to 60 μL mg^{-1} of active material). 0.45 M $Mg(CB_{11}H_{12})_2$/G4 and 0.25 M $Mg[B(hfip)_4]_2$/G4 were used as electrolytes. The assembled Swagelok cells were cycled within the potential window of 0.2–3.3 V versus Mg^{2+}/Mg at a cycling rate of 1C and 0.2C for $Mg(CB_{11}H_{12})_2$/G4 and $Mg[B(hfip)_4]_2$/G4 electrolytes, respectively. All experiments were performed inside the glovebox.

Acknowledgements

This work is funded by the Advanced Research Projects Agency-Energy (ARPA-E), US Department of Energy, under award number DE-AR0001548.

Conflict of Interest

Y.Y. holds equity and consults for LiBeyond, LLC and and Solid Design Instruments, LLC. This financial interest has been disclosed to the University of Houston, and appropriate steps have been taken to address any potential conflicts of interest. A.E.L., Y.L., and Y.Y. have filed a U.S. Provisional Patent (application number 63/551 295) comprising the work described herein. The remaining authors declare that they have no competing interests.

Author Contributions

Yan Yao directed the project. **Alae Eddine Lakraychi** and **Yanliang Liang** designed the experiment. **Alae Eddine Lakraychi** performed the synthesis, characterization, and electrochemical tests. **Leonard Linshin Jiang** performed SEM. **Wen Ren** and **Mark Wayne Lee Jr.** prepared the electrolytes. **Alae Eddine Lakraychi** wrote the first draft of the manuscript. **Yanliang Liang**, **Ye Zhang**, **Wen Ren** and **Yan Yao** revised the manuscript. All authors discussed the results and commented on the manuscript.

Data Availability Statement

The data that support the findings of this study are available from the corresponding author upon reasonable request.

Keywords: bis-benzoquinone · dissolution-precipitation reaction · magnesium batteries · solute-electrolyte interactions

[1] R. Mohtadi, O. Tutusaus, T. S. Arthur, Z. Zhao-Karger, M. Fichtner, *Joule* **2021**, *5*, 581.
[2] H. D. Yoo, I. Shterenberg, Y. Gofer, G. Gershinsky, N. Pour, D. Aurbach, *Energy Environ. Sci.* **2013**, *6*, 2265.
[3] Y. Liang, H. Dong, D. Aurbach, Y. Yao, *Nat. Energy* **2020**, *5*, 646.
[4] C. Ling, D. Banerjee, M. Matsui, *Electrochim. Acta* **2012**, *76*, 270.
[5] D. Aurbach, Z. Lu, A. Schechter, Y. Gofer, H. Gizbar, R. Turgeman, Y. Cohen, M. Moshkovich, E. Levi, *Nature* **2000**, *407*, 724.
[6] J. A. Blázquez, R. R. Maça, O. Leonet, E. Azaceta, A. Mukherjee, Z. Zhao-Karger, Z. Li, A. Kovalevsky, A. Fernández-Barquín, A. R. Mainar, P. Jankowski, L. Rademacher, S. Dey, S. E. Dutton, C. P. Grey, J. Drews, J. Häcker, T. Danner, A. Latz, D. Sotta, M. R. Palacin, J.-F. Martin, J. M. G. Lastra, M. Fichtner, S. Kundu, A. Kraytsberg, Y. Ein-Eli, M. Noked, D. Aurbach, *Energy Environ. Sci.* **2023**, *16*, 1964.
[7] S. Riedel, L. Wang, M. Fichtner, Z. Zhao-Karger, *Chem. – A European J.* **2024**, *30*, e202402754.
[8] H. Zhang, L. Qiao, M. Armand, *Angew. Chem. Int. Ed.* **2022**, *61*, e202214054.
[9] S. Hou, X. Ji, K. Gaskell, P. Wang, L. Wang, J. Xu, R. Sun, O. Borodin, C. Wang, *Science* **2021**, *374*, 172.
[10] C. Li, R. D. Guha, A. Shyamsunder, K. A. Persson, L. F. Nazar, *Energy Environ. Sci.* **2024**, *17*, 190.
[11] D.-T. Nguyen, A. Y. S. Eng, M.-F. Ng, V. Kumar, Z. Sofer, A. D. Handoko, G. S. Subramanian, Z. W. Seh, *Cell Rep. Phys. Sci.* **2020**, *1*, 100265.
[12] O. Tutusaus, R. Mohtadi, T. S. Arthur, F. Mizuno, E. G. Nelson, Y. V. Sevryugina, *Angew. Chem. Int. Ed.* **2015**, *54*, 7900.
[13] Z. Zhao-Karger, M. E. Gil Bardaji, O. Fuhr, M. Fichtner, *J. Mater. Chem. A* **2017**, *5*, 10815.
[14] M. Mao, T. Gao, S. Hou, C. Wang, *Chem. Soc. Rev.* **2018**, *47*, 8804.
[15] M. M. Huie, D. C. Bock, E. S. Takeuchi, A. C. Marschilok, K. J. Takeuchi, *Coord. Chem. Rev.* **2015**, *287*, 15.
[16] Z. Li, J. Häcker, M. Fichtner, Z. Zhao-Karger, *Adv. Energy Mater.* **2023**, *13*, 2300682.
[17] H. D. Yoo, Y. Liang, H. Dong, J. Lin, H. Wang, Y. Liu, L. Ma, T. Wu, Y. Li, Q. Ru, Y. Jing, Q. An, W. Zhou, J. Guo, J. Lu, S. T. Pantelides, X. Qian, Y. Yao, *Nat. Commun.* **2017**, *8*, 339.
[18] G. S. Gautam, P. Canepa, R. Malik, M. Liu, K. Persson, G. Ceder, *Chem. Commun.* **2015**, *51*, 13619.
[19] E. Levi, Y. Gofer, D. Aurbach, *Chem. Mater.* **2010**, *22*, 860.
[20] M. Liu, Z. Rong, R. Malik, P. Canepa, A. Jain, G. Ceder, K. A. Persson, *Energy Environ. Sci.* **2015**, *8*, 964.
[21] E. Levi, M. D. Levi, O. Chasid, D. Aurbach, *J. Electroceram.* **2009**, *22*, 13.
[22] D. Prill, P. Juhás, S. J. L. Billinge, M. U. Schmidt, *Acta Crystallogr. A Found. Adv.* **2016**, *72*, 62.
[23] L. Wang, S. Riedel, J. Drews, Z. Zhao-Karger, *Front. Batteries and Electrochem.* **2024**, *3*, 1358199.
[24] L. Kong, C. Yan, J.-Q. Huang, M.-Q. Zhao, M.-M. Titirici, R. Xiang, Q. Zhang, *Energy & Environ. Mater.* **2018**, *1*, 100.

[25] H. Tian, T. Gao, X. Li, X. Wang, C. Luo, X. Fan, C. Yang, L. Suo, Z. Ma, W. Han, C. Wang, *Nat. Commun.* **2017**, *8*, 14083.
[26] G. Bieker, V. Küpers, M. Kolek, M. Winter, *Commun. Mater.* **2021**, *2*, 37.
[27] S. Drvarič Talian, A. Vizintin, J. Bitenc, G. Aquilanti, A. Randon-Vitanova, M. Gaberšček, R. Dominko, *ChemElectroChem* **2021**, *8*, 1062.
[28] A. Robba, A. Vizintin, J. Bitenc, G. Mali, I. Arčon, M. Kavčič, M. Žitnik, K. Bučar, G. Aquilanti, C. Martineau-Corcos, A. Randon-Vitanova, R. Dominko, *Chem. Mater.* **2017**, *29*, 9555.
[29] P. Poizot, J. Gaubicher, S. Renault, L. Dubois, Y. Liang, Y. Yao, *Chem. Rev.* **2020**, *120*, 6490.
[30] Y. Lu, Q. Zhang, L. Li, Z. Niu, J. Chen, *Chem* **2018**, *4*, 2786.
[31] J. Sun, Y. Fei, H. Tang, J. Bao, Q. Zhang, X. Zhou, *ACS Appl. Energy Mater.* **2024**, *7*, 7592.
[32] Y. Ge, B. Liu, D. Wu, Y. Zhang, S. Tang, H. Jiang, J. Li, H. Zhang, X. Tian, J. Yang, *ACS Energy Lett.* **2025**, *10*, 1615.
[33] J. Xie, Q. Zhang, *Small* **2019**, *15*, 1805061.
[34] H. Dong, Y. Liang, O. Tutusaus, R. Mohtadi, Y. Zhang, F. Hao, Y. Yao, *Joule* **2019**, *3*, 782.
[35] N.-A. Tran, N. Do Van Thanh, M. L. P. Le, *Chem. – A European J.* **2021**, *27*, 9198.
[36] H. Dong, Y. Yao, *in Encyclopedia of Nanomaterials* (First Edition) (Eds.: Y. Yin, Y. Lu, Y. Xia), Elsevier, Oxford **2023**, pp. 550–557.
[37] H. Aso, O. Tutusaus, T. S. Arthur, J. A. Kaduk, R. Mohtadi, *J. Phys. Chem. C* **2023**, *127*, 2855.
[38] Z. Hu, L. Huang, X. Gan, Y. Han, J. Chu, Z. Song, *ACS Appl. Mater. Interfaces* **2024**, *16*, 19014.
[39] H. Dong, O. Tutusaus, Y. Liang, Y. Zhang, Z. Lebens-Higgins, W. Yang, R. Mohtadi, Y. Yao, *Nat. Energy* **2020**, *5*, 1043.
[40] J. Hu, D. Zhang, F. W. Harris, *J. Org. Chem.* **2005**, *70*, 707.
[41] J. C. Walsh, K.-L. M. Williams, D. Lungerich, G. J. Bodwell, *Eur. J. Org. Chem.* **2016**, *2016*, 5933.
[42] Y. Gao, J. Fu, Y. Hu, F. Zhao, W. Li, S. Deng, Y. Sun, X. Hao, J. Ma, X. Lin, C. Wang, R. Li, X. Sun, *Angew. Chem. Int. Ed.* **2024**, *63*, e202403331.
[43] B. E. Love, *Synth. Commun.* **2022**, *52*, 1581.
[44] T. D. Gregory, M. L. Perry, P. Albertus, *J. Power Sources* **2021**, *499*, 229965.
[45] L. Sieuw, A. Jouhara, É. Quarez, C. Auger, J.-F. Gohy, P. Poizot, A. Vlad, *Chem. Sci.* **2019**, *10*, 418.
[46] S. Zheng, D. Shi, T. Sun, L. Zhang, W. Zhang, Y. Li, Z. Guo, Z. Tao, J. Chen, *Angew. Chem. Int. Ed.* **2023**, *62*, e202217710.
[47] T. Yokoji, Y. Kameyama, N. Maruyama, H. Matsubara, *J. Mater. Chem. A* **2016**, *4*, 5457.
[48] E. Pedraza, C. de la Cruz, A. Mavrandonakis, E. Ventosa, R. Rubio-Presa, R. Sanz, S. T. Senthilkumar, P. Navalpotro, R. Marcilla, *Adv. Energy Mater.* **2023**, *13*, 2301929.
[49] H. A. Adeoye, M. Dent, J. F. Watts, S. Tennison, C. Lekakou, *J. Chem. Phys.* **2023**, *158*, 064702.
[50] A. E. Lakraychi, E. S. Picton, Y. Liang, D. L. Shaffer, Y. Yao, *ACS Energy Lett.* **2023**, *8*, 5032.
[51] X. Huang, Z. Wang, R. Knibbe, B. Luo, S. A. Ahad, D. Sun, L. Wang, *Energy Technol.* **2019**, *7*, 1801001.
[52] M. López-Herraiz, E. Castillo-Martínez, J. Carretero-González, J. Carrasco, T. Rojo, M. Armand, *Energy Environ. Sci.* **2015**, *8*, 3233.
[53] M. W. Lehmann, D. H. Evans, *J. Electroanal. Chem.* **2001**, *500*, 12.
[54] V. A. Nikitina, R. R. Nazmutdinov, G. A. Tsirlina, *J. Phys. Chem. B* **2011**, *115*, 668.
[55] S. Bai, B. Kim, C. Kim, O. Tamwattana, H. Park, J. Kim, D. Lee, K. Kang, *Nat. Nanotechnol.* **2021**, *16*, 77.

Manuscript received: May 11, 2025
Revised manuscript received: July 1, 2025
Version of record online: